

## Alpha–alpha potential up to 47.3 MeV bombarding energy

M.N.A. Abdullah <sup>a</sup>, M.S. Sabra <sup>c</sup>, M.M. Rashid <sup>a</sup>, Z. Shehadeh <sup>d,e</sup>,  
M.M. Billah <sup>a</sup>, S.K. Das <sup>b</sup>, M.A. Uddin <sup>a</sup>, A.K. Basak <sup>a,\*</sup>, I. Reichstein <sup>f</sup>,  
H.M. Sen Gupta <sup>g</sup>, F.B. Malik <sup>c,h</sup>

<sup>a</sup> Department of Physics, University of Rajshahi, Rajshahi-6205, Bangladesh

<sup>b</sup> Department of Physics, Shahjalal University of Science & Technology, Sylhet, Bangladesh

<sup>c</sup> Department of Physics, Southern Illinois University, Carbondale, IL 62901, USA

<sup>d</sup> Department of Physics, Applied Science University, Amman 11931, Jordan

<sup>e</sup> Taif Teachers College, Taif, Saudi Arabia

<sup>f</sup> School of Computer Science, Carleton University, Ottawa, ON K1S 5B6, Canada

<sup>g</sup> Department of Physics, University of Dhaka, Dhaka-1000, Bangladesh

<sup>h</sup> Department of Physics, Washington University, St. Louis, MO 63130, USA

Received 4 February 2006; received in revised form 6 June 2006; accepted 22 June 2006

Available online 5 July 2006

### Abstract

Experimental differential cross sections for elastic scattering of two  $\alpha$  particles have been fitted with an  $l$ -independent non-monotonic real potential up to 34.2 MeV (lab) and a complex potential with non-monotonic real part from 35.1 to 47.3 MeV (lab). The calculated phase shifts, in general, agree with those derived from the phase shift analyses of the experimental cross sections. In particular, the  $s$ - and  $d$ -wave phase shifts tend to zero in the limit of zero energy implying the absence of any bound state. Thus,  ${}^8\text{Be}$  is unbound in the potential and the calculated decay width of about 6 eV agrees with the observed one. This potential has its roots in the energy-density functional (EDF) theory with the sudden approximation. In fact, the calculated angular distributions using the derived EDF potential are in reasonable agreement with the experimental data at some energies up to 15.2 MeV (lab). Modifying the Buck, Friedrich and Wheatley (BFW) potential by adding a small repulsive core leads to about the same quality of fits. The modified BFW potential, however, binds  ${}^8\text{Be}$  in Pauli forbidden states, and  $s$ - and  $d$ -wave phase shifts in it tend to  $2\pi$  and  $\pi$ , respectively, in the limit of zero energy.

© 2006 Elsevier B.V. All rights reserved.

\* Corresponding author.

E-mail addresses: [mnaa03@yahoo.com](mailto:mnaa03@yahoo.com) (M.N.A. Abdullah), [akbasak-phy@ru.ac.bd](mailto:akbasak-phy@ru.ac.bd) (A.K. Basak).

PACS: 25.55.Ci; 24.10.Ht; 21.60.-n

Keywords:  $\alpha$ - $\alpha$  optical potentials; Elastic scattering; Energy density functional; Non-monotonic and Woods–Saxon potentials

---

## 1. Introduction

The knowledge of the  $\alpha$ - $\alpha$  interaction is needed in order to provide insights into many nuclear properties such as  $\alpha$ -like states in nuclei, binding energies in  $\alpha$ -matter, the  $\alpha$ -clustering effect in nuclear scattering, etc. The  $\alpha$ - $\alpha$  system has been studied quite extensively both experimentally [1–12] and theoretically [13–42]. Ostensibly, the determination of the interaction potential for this system should be simple. However, despite many investigations, the detailed nature of the  $\alpha$ - $\alpha$  potential is still conceptually incomplete. On the other hand, the  $\alpha$ -particle, with zero spin and isospin, and being very compact with root-mean-square (RMS) radius of about 1.44 fm and tightly bound with a binding energy of 28 MeV, is a natural ingredient for forming cluster-like states in nuclei, particularly the light ones. The study of such cluster-like configurations requires a knowledge of the  $\alpha$ - $\alpha$  potential.

The determination of the  $\alpha$ - $\alpha$  potential has been attempted in many different ways. The lines of investigations such as the generator coordinate method (GCM) [32], the resonating group method (RGM) [19,25,34,35], the orthogonality condition model (OCM) [36] and the folding potential method [26] involve the determination of this potential from nucleon–nucleon interaction. However, none of these investigations prescribes a unique potential that could be used over a broad range of energy. The phase shift analyses of low energy data led Darriulat et al. [2] to propose an  $l$ -dependent non-monotonic potential with a short range repulsion. Using a Gaussian repulsive and attractive real potential, Ali and Bodmer (AB) [16] could fit the derived  $l = 0, 2,$  and  $4$  phase shifts reasonably well from a few keV to about 20 MeV (lab) incident energy using different parameters of the potential for each partial wave. However, in the limit of zero energy, the  $s$ -wave phase shift seems to go to  $2\pi$ , instead of zero as expected from Levinson's theorem [43]. The  $l$ -dependence of this potential makes it difficult to extrapolate it to higher energies, since higher partial waves start contributing to cross sections at these energies. The  $l$ -independent phenomenological potential of Neudatchin et al. [20] met with limited success. Surprisingly, Buck, Friedrich and Wheatley (BFW), with their  $l$ -independent potential, could reproduce the energy dependence of the  $l = 0, 2, 4$  and  $6$  phase shifts reasonably well, up to about 40 MeV (lab) bombarding energy using a simple strong attractive energy-independent potential of Gaussian shape, provided a phase of  $2\pi$  and  $\pi$  are added to  $l = 0$  and  $l = 2$  phase shifts, respectively. This potential, thus, not only binds  ${}^8\text{Be}$  in two  $s$ -states including the ground state, but also in an excited  $d$ -state, which contradicts the fact that  ${}^8\text{Be}$  is unbound. Noting that the proton, neutron, and  $(p + {}^3\text{He})$  production thresholds in the  $\alpha$ - $\alpha$  scattering are, respectively, 34.73, 38.03, and 39.68 MeV (lab), one expects a loss of flux in these channels, making it necessary to use a complex potential to analyze the elastic scattering data around these and higher bombarding energies. The phase shift analyses at these energies, however, were done assuming them to be real and the BFW potential did not have an imaginary component in it. In fact, the  ${}^4\text{He}(\alpha, p){}^7\text{Li}$  experiment at 38.5 MeV (lab) incident energy [44] indicates a reaction cross section of at least 44 mb at that energy. In their attempt to determine the  $\alpha$ -nucleus potential, Abdullah et al. [45,46], noted that by adding of a small repulsive part to the BFW potential and replacing its Coulomb part by the one due to a uniform charge distribution, one can obtain good

fits to the elastic scattering data of  $\alpha$  particles by  $^{16}\text{O}$  and  $^{40,44,48}\text{Ca}$ . The latter potential is referred to as the BFW potential with a repulsive core (BFWC). The double folding (DF) potential method [26] using the M3Y effective potential of [47] generates a deep potential very similar to BFW and provides good fits to the  $\alpha$ - $\alpha$  scattering data up to about 30 MeV as shown in [14]. However, *the  $\alpha$  density distribution used in the calculation does not bind  $\alpha$ -particle* in the energy-density functional (EDF) formalism.

The aim of this investigation is to search for an  $l$ -independent potential, that has no bound state, provides the correct decay widths of  $^8\text{Be}$  in the ground state, and accounts for the differential elastic scattering and reaction cross sections up to 47.3 MeV (lab). To this end, we shall first determine the general shape of the real part of the  $\alpha$ - $\alpha$  potential using the EDF approach in the sudden approximation [48,49]. Such a procedure has been successful in determining the  $\alpha$ - $^{28}\text{Si}$  [50],  $\alpha$ -Ca [51], and  $\alpha$ -Ni [52] potentials. Once, the general nature of the potential is obtained from the EDF calculation, its parameters are adjusted to reproduce angular distributions. Since  $\alpha$  particles do not have an excited state and the particle production thresholds start around 34.73 MeV (lab), it is expected that the data up to about that energy are amenable to analysis using only a real potential. This is supported by experiments observing no reaction cross section up to about 34.2 MeV [2]. The angular distributions above 34.2 MeV (lab) have been analyzed using a complex potential that accounts for the reaction cross section of at least 44 mb at 38 MeV (lab), as mentioned earlier.

Since the BFW potential and its variation BFWC have been successful in reproducing the data up to about 34.2 MeV (lab), despite the problem near zero energy, we have compared our results with those obtained using these two potentials, as well as a similar potential with Woods–Saxon functional form.

In the next section, we present the outline of the EDF theory to determine the general structure of the  $\alpha$ - $\alpha$  potential, followed by a section on the nature of the empirical potentials used in our search and sections on the search procedure employed, results of analyses and conclusions arrived at. All energies in the subsequent paragraphs are in the laboratory system, unless otherwise noted.

## 2. The energy density functional formalism

In the EDF formalism [48–50], the potential  $V(R)$  between the projectile  $\alpha$  and the target  $\alpha$  at a separation distance  $R$  is given by

$$V(R) = E[\rho(\mathbf{r}, R)] - E[\rho_\alpha(\mathbf{r}, R = \infty)] - E[\rho_T(\mathbf{r}, R = \infty)], \quad (1)$$

where  $\rho$  is the density function of the composite system.  $\rho_\alpha$  and  $\rho_T$  are, respectively, the density functions for the projectile  $\alpha$  and the target  $\alpha$  at  $R = \infty$ . The first, second and third terms on the right side of (1) are, respectively, the total energies of the composite system with the colliding partners at a distance of  $R$ , and of the incident  $\alpha$  particle and the target when they are far apart. The density functions are dependent on the respective position vectors  $\mathbf{r}$  and assumed spherically symmetric. Each of the total energy terms being integral over  $\mathbf{r}$  (see Eq. (5) below), is independent of it. In the sudden approximation, the density distribution function of the composite system is given by

$$\rho(r) = \rho_\alpha(r) + \rho_T(r). \quad (2)$$

The density function of the  $\alpha$  particle,  $\rho_\alpha$ , is reasonably described by the following expression:

$$\rho_\alpha(r) = 4 \left( \frac{\gamma}{\pi} \right)^{3/2} \exp(-\gamma r^2). \quad (3)$$

This is a special case of the generalized bottle Gaussian shape of Elton [53], for a nucleus with atomic number  $Z$ , expressed as

$$\rho(r) = \left( \frac{\gamma}{\pi} \right)^{3/2} \frac{8}{Z} \left( 1 + \left( \frac{Z-2}{3} \right) \gamma r^2 \right) \exp(-\gamma r^2). \quad (4)$$

Eq. (3) leads to the central density and the RMS radius as  $\rho_0 = 4(\gamma/\pi)^{3/2}$  and  $R_{\text{rms}} = (1.5/\gamma)^{1/2}$ , respectively. The total energy  $E$  of the composite system, for the density distribution  $\rho(\mathbf{r})$ , is given [49] by

$$E = \int \epsilon[\rho(\mathbf{r})] d^3\mathbf{r}, \quad (5)$$

where

$$\begin{aligned} \epsilon[\rho(\mathbf{r})] = & 0.3 \left( \frac{\hbar^2}{2M} \right) \left( \frac{3\pi^2}{2} \right)^{2/3} \rho^{5/3} [(1-x)^{5/3} + (1+x)^{5/3}] \\ & + \nu(\rho, x)\rho + \frac{e}{2} \Phi_C(\mathbf{r})\rho_P - 0.739e^2\rho_P^{4/3} + \left( \frac{\hbar^2}{8M} \right) \eta(\nabla\rho)^2. \end{aligned} \quad (6)$$

In the above equation,  $x = (N - Z)/A$  is the neutron excess parameter, which is zero for the  $\alpha$ - $\alpha$  system and  $M$  is the nucleon mass.  $\Phi_C$  and  $\rho_P$  are, respectively, the Coulomb potential and the proton density function. The last term in  $\eta$  is the correction to the kinetic energy due to non-uniform density distribution and the total energy due to correlation not included in the mean field.  $\eta$  is the free parameter adjusted to reproduce the observed nuclear masses from the  $\alpha$  particle to uranium.  $\nu(\rho, x)$  is the average potential of a nucleon in a nuclear matter which has been calculated in [54] from a realistic two-nucleon potential in the Brueckner–Hartree–Fock approximation. This means that the potential is calculated evaluating both direct and exchange terms of  $T$ -matrices and as such it includes contributions from the Pauli exchange effect. The density dependence of the average potential is given by

$$\nu(\rho, x) = b_1(1 + a_1x^2)\rho + b_2(1 + a_2x^2)\rho^{4/3} + b_3(1 + a_3x^2)\rho^{5/3}, \quad (7)$$

with  $b_1 = -741.28$ ,  $b_2 = 1179.89$  and  $b_3 = -467.54$ . Since  $x$  is zero for  $\alpha$  particles, the values of  $a_1$ ,  $a_2$  and  $a_3$  are immaterial. The Coulomb potential  $\Phi_C$  in (6) is related to the proton density distribution  $\rho_P$  as

$$\Phi_C = e \int \frac{\rho_P(\mathbf{r}')}{|\mathbf{r} - \mathbf{r}'|} d^3\mathbf{r}'. \quad (8)$$

The fourth term in (6) is the correction to the Coulomb potential due to the Pauli principle operating among the protons.

Thus, the potential calculated using (1) is derived from a realistic two-nucleon interaction with the inclusion of the Pauli principle among neutrons and protons. The observed masses of a range of nuclei can be accounted for within 1.5% using the observed density distribution functions, i.e. with the observed RMS radii [55].

### 3. Analysis and discussion

Experimental differential cross sections of elastic scattering data are available over the energy range of 150 keV to 650 MeV [1–12]. However, we have analyzed here the data up to 47.3 MeV only because the experimental total reaction cross sections increase substantially [2] at higher energies implying that the absorption plays a significant role. Such a significant change in the imaginary part of the potential is likely to influence the nature of the real part substantially because of the dispersion relation between them [56,57]. As noted earlier, the analysis of the data up to about 34.2 MeV may not need any imaginary part. At higher energies, a few other reaction channels open up requiring a modest imaginary part in analyses resulting in a slight change of the parameters of the real part.

#### 3.1. Parametrization of the EDF, BFW and BFWC potentials

The EDF calculations are performed using the parameter  $\eta = 7.56 \text{ fm}^3$  in (6). The use of the width parameter  $\gamma = 0.58$  leads to the  $\alpha$  central density of  $\rho_0 = 0.317 \text{ fm}^{-3}$ , the RMS radius,  $R_{\text{rms}} = 1.608 \text{ fm}$  and the binding energy  $\text{BE} = 12.93 \text{ MeV}$ . The latter is significantly lower than the experimental one. On the other hand, the value of  $\gamma = 0.45$  yields  $\rho_0 = 0.217 \text{ fm}^{-3}$ ,  $R_{\text{rms}} = 1.825 \text{ fm}$  and  $\text{BE} = 20.96 \text{ MeV}$ . Although the BE is reasonable, the central density is too low compared to the deduced value of  $0.32 \text{ fm}^{-3}$  from experiments.  $\gamma = 0.5$  is taken as a good compromise leading to  $\rho_0 = 0.254 \text{ fm}^{-3}$ ,  $R_{\text{rms}} = 1.732 \text{ fm}$  and  $\text{BE} = 19.01 \text{ MeV}$  with  $R_{\text{rms}}$  close to the range  $R_{\text{rms}} = 1.67\text{--}1.70 \text{ fm}$ , as quoted in the compilation of de Vries et al. [58]. Various forms of the nuclear density distributions for  $\alpha$  particles have been tried by Avrigeanu et al. [14] to analyze the  $\alpha\text{--}\alpha$  scattering data in incident energy range 8.87–29.5 MeV in terms of the DF potential of the M3Y interactions. Only the density distributions of Love and Satchler (DDLs) [26], and Baye et al. (DDB) [59] could generate appropriate folding potentials to reproduce the best possible descriptions of the data. Both DDLs and DDB have the density distributions similar to the form in Eq. (3) with the width parameters  $\gamma = 0.7024$  and  $0.8138$ , respectively. The latter two  $\gamma$  values in the EDF calculations lead to *unbound*  $\alpha$  particles.

The  $\alpha\text{--}\alpha$  potential, determined from the EDF calculations with  $\gamma = 0.5$  in (3), is shown as solid dots in Fig. 1. The key feature of this potential is that it is non-monotonic with a short-range repulsion followed by an attractive part. We present two functions to reproduce these calculated points. The chosen functional representations of these calculated potential points, dictated by the motivation to fit the data by varying the parameters, are real parts of the following:

$$V_{\text{GG}}(r) = -V_A \exp\left(-\frac{r^2}{R_A^2}\right) + V_R \exp\left(-\frac{r^2}{R_R^2}\right) - iW_0 \exp\left(-\frac{r^2}{R_W^2}\right) + V_C(r) \quad (9)$$

and

$$V_{\text{WG}}(r) = -V_0 \left[ 1 + \exp\left(\frac{r - R_0}{a_0}\right) \right]^{-1} + V_R \exp\left(-\frac{r^2}{R_R^2}\right) - iW_0 \exp\left(-\frac{r^2}{R_W^2}\right) + V_C(r). \quad (10)$$

The first term in each of (9) and (10) represents the real attractive part in the Gaussian and Woods–Saxon (WS) forms, respectively. The second term of both the equations denotes the real repulsive part in the Gaussian form. The third term is the imaginary part again with the Gaussian

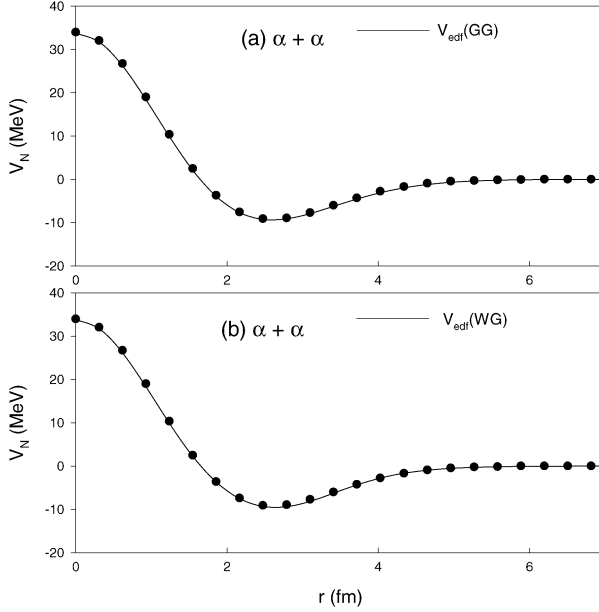


Fig. 1. Real nuclear part of the  $\alpha$ - $\alpha$  potential, computed from the EDF theory, shown in solid dots, is parametrized by the (a)  $V_{\text{edf}}(\text{GG})$  using the Gaussian attractive and Gaussian repulsive geometries in the upper insert, and (b)  $V_{\text{edf}}(\text{WG})$  function, using the WS attractive and Gaussian repulsive form-factor in the lower insert. The functional values are shown in solid lines.

form. The fourth term is the Coulomb potential which is taken to be that of a uniformly charged sphere:

$$\begin{aligned}
 V_C(r) &= \left[ \frac{Z_1 Z_2 e^2}{2R_C} \right] \left[ 3 - \frac{r^2}{R_C^2} \right] \quad \text{for } r \leq R_C, \\
 &= \frac{Z_1 Z_2 e^2}{r} \quad \text{for } r > R_C.
 \end{aligned} \tag{11}$$

In (11),  $Z_1 = Z_2 = 2$  for the  $\alpha$ - $\alpha$  scattering. These fundamental forms of the potential have been successful in describing  $\alpha$ -scattering by Ca [51], Ni [52], Mg and Si [60].

The calculated  $\alpha$ - $\alpha$  potentials, obtained from the EDF theory, are parametrized using the real part of both the functional forms in (9) and (10), and are noted in Table 1 as the  $V_{\text{edf}}(\text{GG})$  and  $V_{\text{edf}}(\text{WG})$  sets. The former set, with the attractive part in the Gaussian form, has a volume integral  $J_R/16 = -119.7 \text{ MeV fm}^3$ , while the latter with the WS geometry bears the integral value  $J_R/16 = -112.4 \text{ MeV fm}^3$ . These two sets provide the initial parameters to analyze the experimental data.  $V_{\text{edf}}(\text{GG})$  and  $V_{\text{edf}}(\text{WG})$  are attempts to represent the same potential using two different functions. The sharp differences in magnitude of the attractive and repulsive parts have no particular significance since both of them yield approximately *the same total potential* which determines the scattering amplitudes and the slight disagreement in the volume integrals simply reflects the difference in the approximations involved in the fitting procedure. Within the framework of the calculated potential using the EDF theory, we have attempted to fit the data from a few tens of keV to 47.3 MeV by varying the parameters of the potentials (9) and (10). In the search for reasonable fits, attention has primarily been paid to enhance the repulsive

Table 1

Parametrization of the EDF generated potential and the fit parameters for non-monotonic shallow (NMS) potential sets. All the sets have  $R_C = 5.8$  and  $R_W = 2.0$  fm, where applicable. The parameters  $V_0$  and  $R_0$  are applicable to the WS attractive real part while  $V_A$  and  $R_A$ , to the Gaussian attractive real one.  $V_0$ ,  $V_A$ ,  $V_R$  and  $W_{00}$  are in MeV;  $R_0$ ,  $R_A$ ,  $R_R$  and  $a_0$ , in fm; and  $J_R/16$  and  $J_I/16$ , in MeV fm<sup>3</sup>.  $W_0 = W_{00}[1 + C_1 E_\alpha]$  with  $c_1$  in MeV<sup>-1</sup>

Set	$E_\alpha$	$V_0/V_A$	$R_0/R_A$	$a_0$	$V_R$	$R_R$	$W_{00}$	$C_1$	$J_R/16$	$J_I/16$
$V_{\text{edf}}(\text{GG})$	–	127.6	2.20	–	161.3	1.846	–	–	–119.7	–
$V_{\text{edf}}(\text{WG})$	–	15.56	3.25	0.492	49.24	1.510	–	–	–112.4	–
NMS-1	2.0–9.88	15.40	3.95	0.40	150.0	1.68	–	–	–26.1	–
NMS-1a	2.0–9.88	13.05	3.85	0.61	80.0	1.68	–	–	–111.2	–
NMS-2	12.3–34.2	20.00	3.95	0.10	150.0	1.60	–	–	–110.9	–
NMS-3	35.1–38.83	20.00	3.95	0.90	220.0	1.60	1.613	0.3	+781.6	–(28.2–30.7)
NMS-2	40.77–47.28	20.00	3.95	0.10	150.0	1.60	1.613	0.3	–110.9	–(32.0–36.4)

parameter  $V_R$  followed by an adjustment of other parameters including the depth of the attractive part, either  $V_A$  in (9) or  $V_0$  in (10). This is because the EDF potential parameters have been generated using the width parameter  $\gamma = 0.5$ , which does not adequately reproduce the correct central density of about  $\rho_0 = 0.32$  fm<sup>-3</sup> of  $\alpha$ -particles, and thus, may not have generated enough strength for the repulsive core. In fitting the cross section data, due attention has been given to reproduce the experimental phase shifts  $\delta_0$ ,  $\delta_2$  and  $\delta_4$ . Since the total reaction cross section  $\sigma_R$  has been observed [2] to be zero up to the particle production threshold, the imaginary part has been set to zero up to  $E_\alpha = 34.2$  MeV. The potential determined from the EDF calculations should only be valid up to this energy.

The BFW potential is not non-monotonic. It is a deep potential of Gaussian type without any imaginary part, i.e. it is of the type (9) with  $V_R$  and  $W_0$  being set to zero and has the following form for the Coulomb potential.

$$V_C^{\text{BFW}}(r) = (4e^2) \text{erf}(\beta r)/r, \quad (12)$$

with  $\text{erf}(\beta r) = \frac{2}{\sqrt{\pi}} \int_0^{\beta r} \exp(-t^2) dt$  and  $\beta = 0.75$  fm<sup>-1</sup>.

The BFWC potential is also deep and has the functional form of Eq. (9) with the Coulomb potential given by Eq. (11).

### 3.2. The phenomenological determination of potential parameters

The parameters of the potentials have been determined by fitting the elastic scattering data using both visual and chi-square criteria. A set of parameters is obtained by minimizing the  $\chi^2$  defined by

$$\chi^2 = \frac{1}{(N - F)} \sum_i \left[ \frac{\sigma_{\text{exp}}(\theta_i) - \sigma_{\text{th}}(\theta_i)}{\Delta \sigma_{\text{exp}}(\theta_i)} \right]^2, \quad (13)$$

where  $\sigma_{\text{exp}}(\theta_i)$  and  $\Delta \sigma_{\text{exp}}(\theta_i)$  are, respectively, the experimental cross section and its error at the scattering angle  $\theta_i$ .  $\sigma_{\text{th}}(\theta_i)$  is the calculated cross section generated from the optical potential.  $N$  is the number of data points for the given incident energy and  $F$  is the number of adjusted parameters at the corresponding energy. The quality of fits is judged by the total  $\chi_T^2$ -value defined by

$$\chi_T^2 = \sum_i (\chi^2)_i, \quad (14)$$

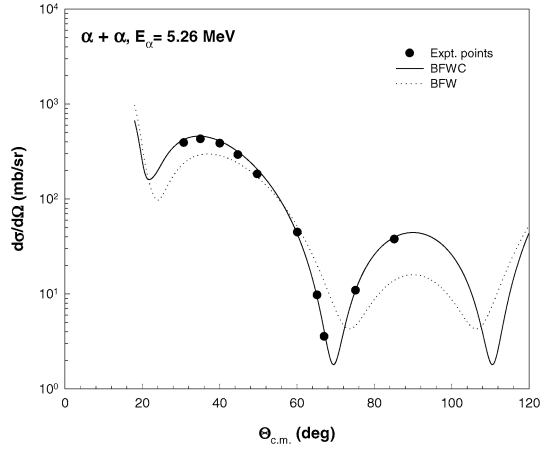


Fig. 2. Computed cross sections of the  $\alpha$ - $\alpha$  scattering at 5.26 MeV using the BFW (dotted line) and BFWC (solid line) potentials are compared with the experimental data in solid dots.

Table 2

Parameters of the deep potential sets. All the sets have  $R_C = 5.8$  and  $R_W = 2.0$  fm.  $V_0/V_A$ ,  $V_R$  and  $W_0$  are in MeV;  $R_0/R_A$ ,  $R_R$  and  $a_0$ , in fm; and  $J_R/16$  and  $J_I/16$ , in MeV fm<sup>3</sup>

Set	$E_\alpha$	$V_0/V_A$	$R_0/R_A$	$a_0$	$V_R$	$R_R$	$W_0$	$J_R/16$	$J_I/16$
BFW	2.0–34.2	122.62	2.132	–	–	–	–	–413.6	–
BFWC	2.0–34.2	122.62	2.132	–	3.0	2.0	–	–405.2	–
BFWC	35.1–38.83	122.62	2.132	–	3.0	2.0	3.9	–405.2	–10.86
BFWC	40.77–47.28	122.62	2.132	–	20.0	2.0	3.9	–357.9	–10.86
WS	2.0–34.2	129.2	1.70	0.65	–	–	–	–410.0	–

where  $i$  runs over all the energy points. The data have been analyzed using the optical model code SCAT2 [61] which has been modified to properly antisymmetrize the two identical bosons. For fitting the angular distributions, the chi-square minimization code MINUIT [62] has been used in conjunction with SCAT2. For analyzing data at energies below 3.0 MeV, the code HARD-CORE [63] has been employed. At higher energies, the calculated cross sections from SCAT2 and HARD-CORE have been found to agree.

### 3.2.1. Deep potential

Despite the problem with the BFW potential near zero energy, mentioned earlier, and the fact that it binds  $^8\text{Be}$  both in the ground and excited states, we have investigated its role in explaining the angular distributions up to 47.3 MeV. Although it reproduces these angular distributions reasonably well, improved fits can be achieved by adding a small repulsive part to it and using the Coulomb potential (11) due to a uniform charge distribution instead of (12) leading to the BFWC potential, as defined earlier. In particular, the fit to the data at 5.26 MeV, using BFW, improves significantly if one uses BFWC, as can be seen in Fig. 2. Similarly, the chi-square of the fit to the 15.2 MeV data are  $\chi^2 = 16.9$  and 3.70, respectively, for the BFW and BFWC potentials. The total  $\chi^2$  in the energy range of 2.0 to 34.2 MeV using BFWC is  $\chi_T^2 = 170.60$ , which is much lower than  $\chi_T^2 = 482.26$  using BFW. This indicates a preference to use the former rather than the latter potential set. The BFW and BFWC parameters are noted in Table 2 and

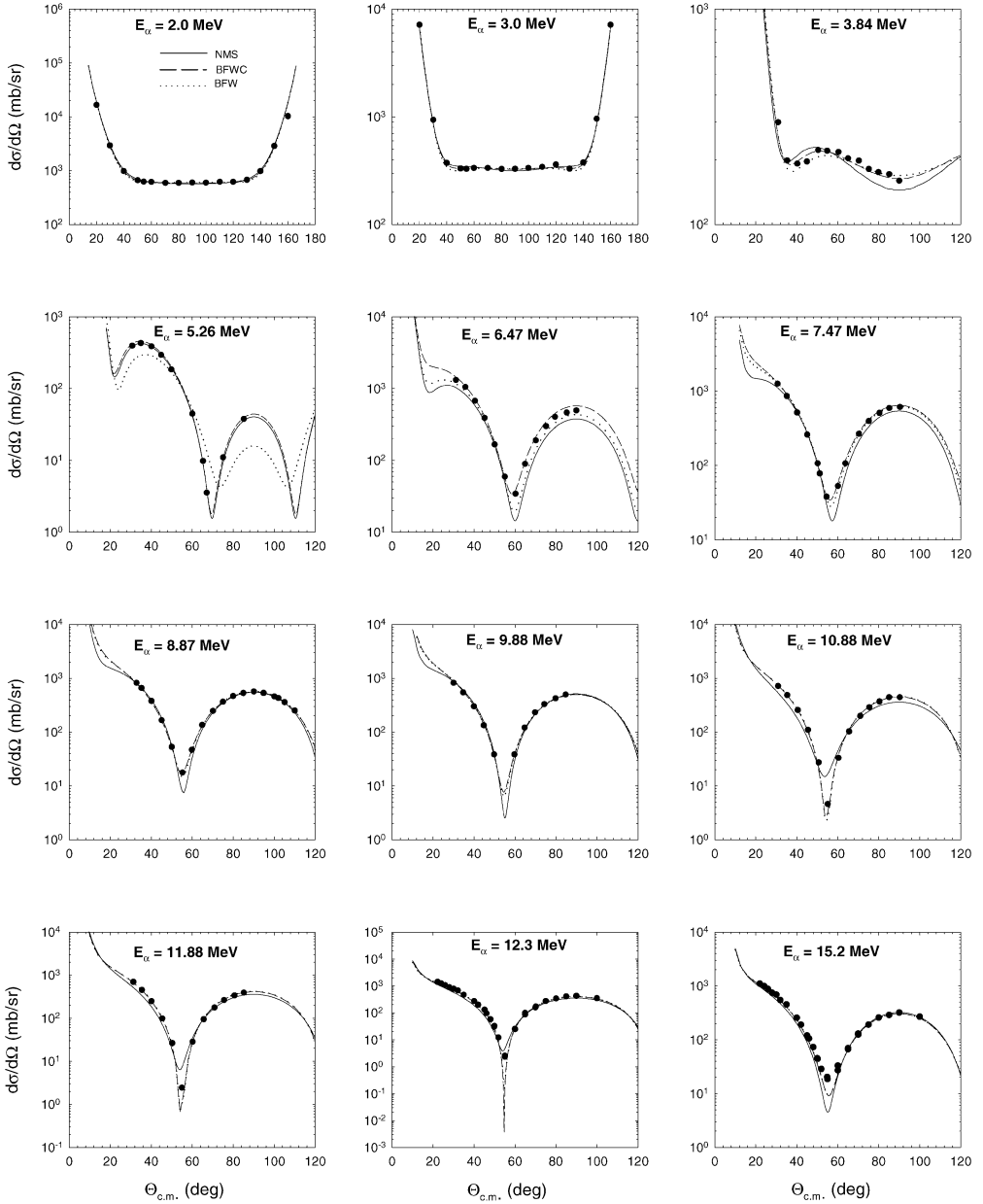


Fig. 3. Computed angular distributions of the  $\alpha$ - $\alpha$  scattering in energy range 2.0–15.2 MeV (lab) using the (i) NMS (solid lines), (ii) BFW (dotted lines) and (iii) BFWC (dashed lines) are compared to the data. The NMS parameters are noted in Table 1 and those of BFW and BFWC, in Table 2. The experimental data are from [4–6].

the predicted angular distributions are compared to the data in Figs. 3–5. Beyond 34.2 MeV, it is necessary to add an imaginary component to this potential. The data in the range from 35.1 to 42.3 MeV are, however, well fitted by adding a Gaussian imaginary component having a depth

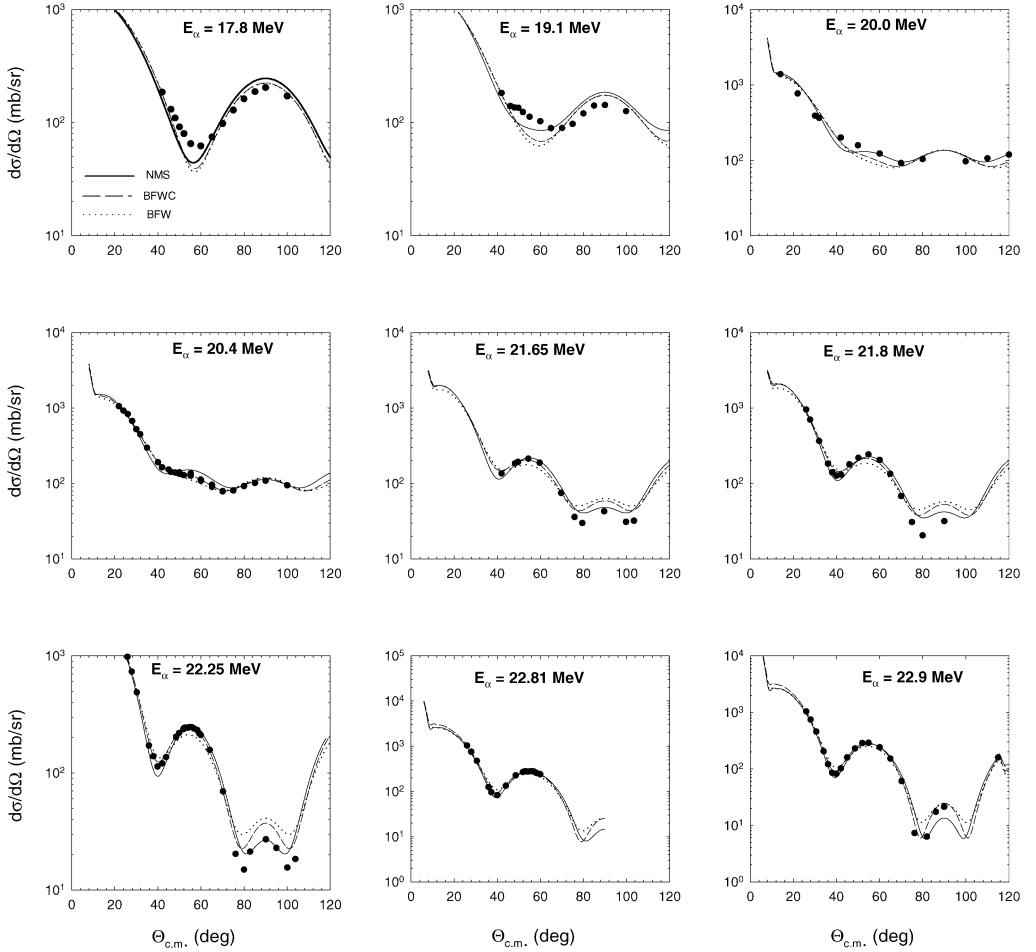


Fig. 4. Same as in Fig. 3 for the incident energy range 17.8–22.9 MeV (lab). The experimental data are from [4].

of 3.9 MeV and a range of 2.0 fm to the BFWC potential, as noted in Table 2. The predicted angular distributions are compared to the data in Fig. 6.

The nuclear part of the BFW and BFWC potential can be approximated to a WS potential,  $-V_0/(1 + \exp[(r - R_0)/a_0])$ , with  $V_0 = 129.2$  MeV,  $R_0 = 1.7$  fm and  $a_0 = 0.65$  fm. Since this potential function is akin to BFWC, the fits using this WS potential are about the same as BFW and BFWC. This WS potential is also close to that in Neudatchin et al. [20]. The BFW, BFWC and the WS potentials are shown in Fig. 7.

### 3.2.2. Non-monotonic shallow (NMS) potential

Using the two parametrized potential functions,  $V_{\text{edf}}(\text{GG})$  and  $V_{\text{edf}}(\text{WG})$  of the actually calculated potential obtained from the EDF theory, we have first predicted the angular distributions at a number of energies up to about 15 MeV and compared them with the experimental data. These are presented in Fig. 8. Amazingly enough, the theory, which has its root in the realistic two-nucleon potential, could account for the data very well at a number of energies with some

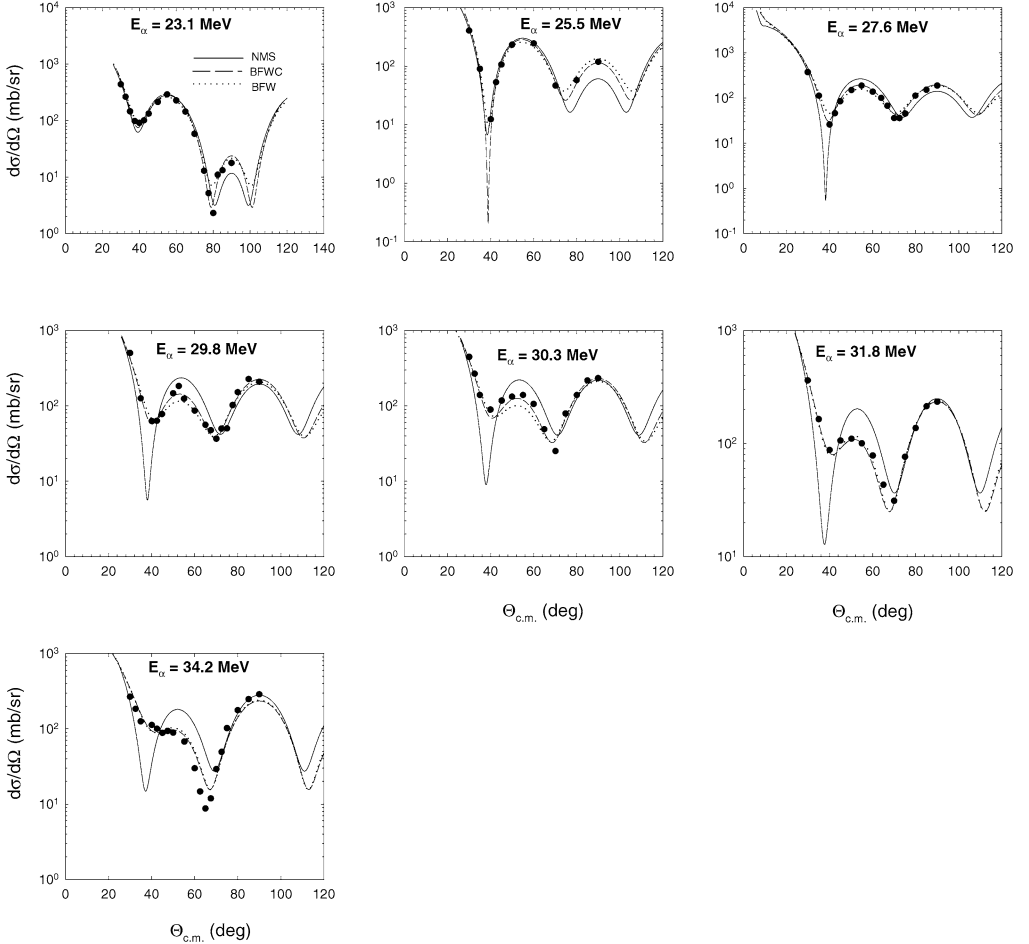


Fig. 5. Same as in Fig. 3 for the incident energy range 23.1–34.2 MeV (lab). The experimental data are from [8].

significant exceptions. Both  $V_{\text{edf}}(\text{GG})$  and  $V_{\text{edf}}(\text{WG})$  reproduce the 2.0 and 3.0 MeV data. This implies that the s-wave phase shifts at these energies can be accounted for by them, since this is the only partial wave contributing to cross sections at these energies. The failure to account for the data between 3.84 and 10.88 MeV by both the  $V_{\text{edf}}(\text{GG})$  and  $V_{\text{edf}}(\text{WG})$  potentials indicates that the d-wave threshold responsible for the dip around  $60^\circ$  is not very well accounted for by them. The ability of both potentials to account for the data at a number of higher incident energies implies that the general structure of the actual potential is given by these two functional forms. However,  $V_{\text{edf}}(\text{WG})$  seems to be slightly better in fitting the data and we, therefore, choose this functional form to search for parameters to fit the data. This latter potential set also has an extra parameter providing more flexibility in fitting the data.

At low energies, e.g. less than 10 MeV, the detailed nature of the Coulomb potential is likely to influence the calculations. Neither the function (11) nor (12) may represent the actual situation. In particular, at very low energies the polarization of the Coulomb potential due to the electrostatic interaction between two  $\alpha$ -particles may influence their interaction pattern. Such a change in the

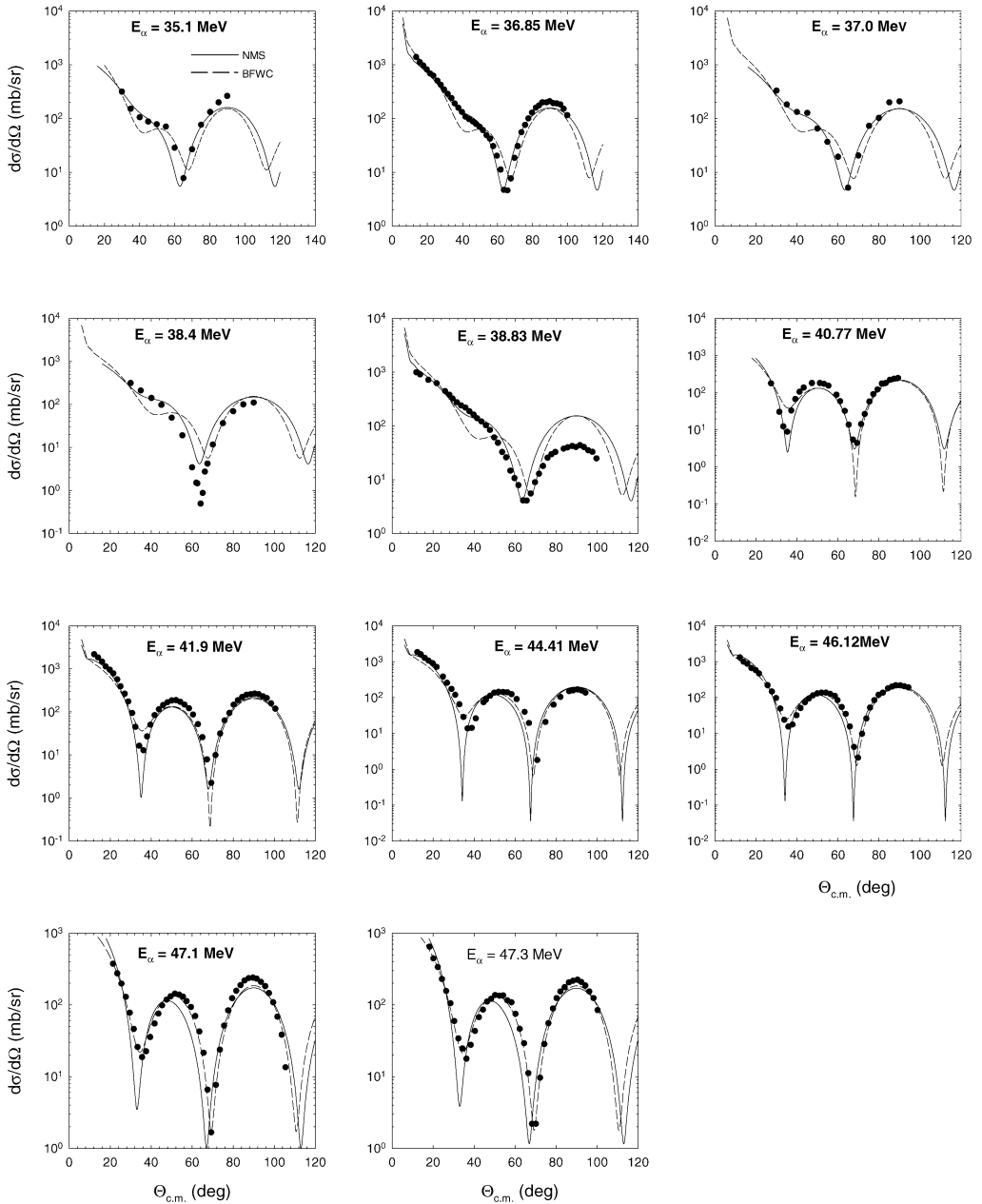


Fig. 6. Same as in Fig. 3 for the incident energy range 35.1–47.3 MeV using the (i) NMS (solid lines) and (ii) BFWC (dashed lines) potentials. The experimental data are from [8,9].

Coulomb potential affects the total potential, e.g. the sum of the Coulomb and nuclear parts of the  $\alpha$ – $\alpha$  potential. This latter situation could also be concocted by keeping the Coulomb potential unchanged but changing the parameters of the nuclear part. Attempts to find a good fit to the data from about zero to 47.3 MeV, indeed, require a slight modification of the parameters in different

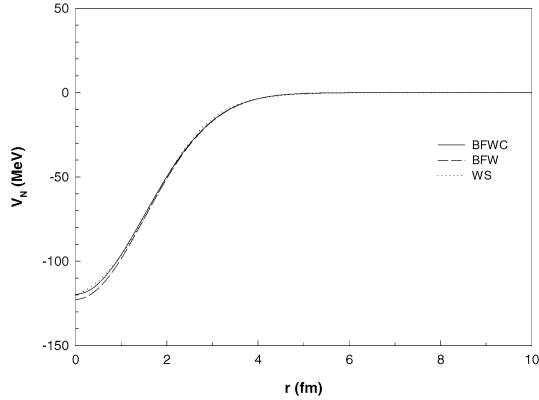


Fig. 7. Comparison of the real nuclear parts of the BFW (broken line), BFWC (solid line) and WS (dotted line)  $\alpha$ - $\alpha$  potentials. The parameters are noted in Table 2.

energy-bins, the polarization effect being dominant at lower energies than at higher ones. This approach leads to what we are referring to in Table 1 as the NMS potential sets.

The fits to the data between 2.0 and 9.88 MeV using NMS-1 are shown in Fig. 3, as solid lines, and the corresponding parameters are noted in Table 1. The data at 2.0 and 3.0 MeV are basically isotropic between  $50^\circ$  to  $130^\circ$  implying that the s-wave is the primary contributor to the scattering which is indeed the case. On the other hand, the data at 5.26 MeV is indicative of a significant contribution from the d-wave. The fits to the data at this energy range using NMS-1 ( $\chi_T^2 = 14.78$ ) are much better than the one with BFW ( $\chi_T^2 = 33.26$ ) and slightly inferior than that with BFWC ( $\chi_T^2 = 4.08$ ).

The fits to the data between 10.88 and 34.2 MeV for the NMS, BFWC and BFW potential sets are also shown in Figs. 3–5. The parameters of the NMS potential in this energy range, referred as the NMS-2 set, are slightly different from those used at the lower energies (NMS-1), as indicated in Table 1. The quality of the fits using the NMS potential is again satisfactory and the total  $\chi^2$  for the fits,  $\chi_T^2 = 869.8$ , for the NMS case is, however, not as good as that using BFWC with  $\chi_T^2 = 164.5$ . Since neither NMS nor BFWC has an imaginary component, the total reaction cross section in each case is zero at all energies in this interval as seems to be the case experimentally [2].

For monotonic deep potentials, it has been customary to calculate volume integrals to distinguish the families of potentials [64]. For NMS potentials, there could be a large cancellation between the positive and negative parts of the volume integral which might make it difficult to use this as a criterion to designate a particular potential family. The problem is exemplified by observing that the volume integrals of the two potentials,  $V_{\text{edf}}(\text{WG})$  and  $V_{\text{edf}}(\text{GG})$  calculated from the EDF theory and noted in Table 1, are  $J_R/16 = -112.4$  and  $-119.7 \text{ MeV fm}^3$ , where as the NMS-1 set again in Table 1 has  $J_R/16 = -26.1 \text{ MeV fm}^3$ . This is because the strength of the repulsive part of NMS-1 is significantly higher than those of  $V_{\text{edf}}(\text{WG})$  and  $V_{\text{edf}}(\text{GG})$ . However, almost a similar quality of fits could be achieved by changing the parameters of set-1. The changed parameters of the resulting new NMS set (NMS-1a), in Table 1, yield the volume integral  $J_R/16 = -111.2 \text{ MeV fm}^3$  which is close to  $J_R/16 = -110.0$  for the NMS-2 set. The volume integral of NMS-1a is more negative than NMS-1, simply because of the reduction in the magnitude of the repulsive part, which does not significantly affect the fits to the data at low energies. In fact, the fits to the cross sections up to 9.88 MeV, which is primarily determined by

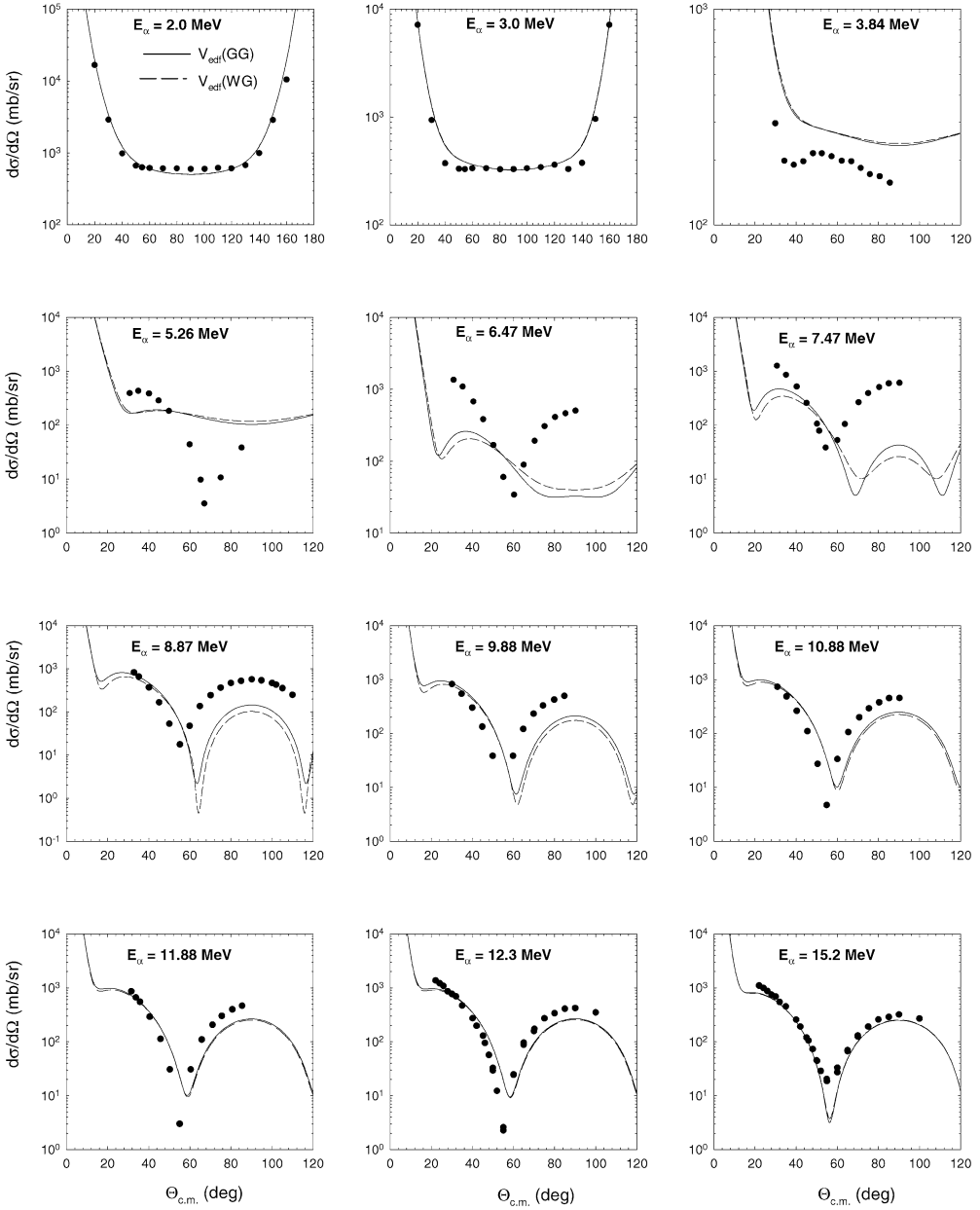


Fig. 8. Comparison of the experimental  $\alpha$ - $\alpha$  angular distributions for 2.0–15.2 MeV (lab) incident energies with the predictions using the parametrized potentials  $V_{\text{edf}}(\text{GG})$  and  $V_{\text{edf}}(\text{WG})$  of the actual one obtained from the EDF calculation. The parameters are noted in Table 1.

the exterior part of the potential, are about the same as those obtained using NMS-1 of Table 1. The total  $\chi^2$  for the fits using NMS-1 in the energy range 2.0–9.88 MeV,  $\chi_T^2 = 14.78$ , is only slightly better than  $\chi_T^2 = 23.66$  using NMS-1a.

Table 3

Reaction cross sections  $\sigma_R$  for the bombarding energies in the range  $E_\alpha(\text{lab}) = 35.1\text{--}47.3$  MeV from the NMS and BFWC potential parameters in Tables 1 and 2, respectively. NMS refers to the NMS-3 set from 35.1 to 38.83 MeV and NMS-2 at higher energies

$E_\alpha$ (MeV)	$\sigma_R$ (mb)	
	NMS	BFWC
35.1	40.6	427.0
36.85	43.1	392.0
37.0	43.4	389.0
38.4	45.4	367.0
38.83	46.0	361.0
40.77	326.0	370.0
41.9	329.0	355.0
44.41	339.0	326.0
46.12	349.0	310.0
47.1	356.0	302.0
47.3	358.0	300.0

As noted earlier, a number of particle production, as well as inelastic channels, are open above 34.2 MeV, and hence, one needs to analyze the data with a complex potential. The conservation of flux leads to the dispersion relation that connects a class of real and imaginary potentials [56, 57]. Thus, the onset of the imaginary potential affects the strength of the real part of the potential. However, the inelastic scattering measurement in [44] indicates the total reaction cross section to be small, probably about a few tens of millibarn.

The fits to the data between 35.10 and 38.83 MeV are not very good using the NMS-2 set. However, an improved fit could be obtained using the parameters NMS-3 which is also listed in Table 1. The calculated total reaction cross sections are 40.6 and 46.0 mb, respectively, at 35.1 and 38.83 MeV (Table 3). The latter value is in line with the measured inelastic cross section of 44 mb at 38.5 MeV, noting that the total reaction cross section should be larger than this. On the other hand, the data based phase shift analysis around 35 MeV indicates a sudden jump at this energy [2] implying the occurrence of a resonance. Furthermore, the presence of a resonance makes the parameters of the NMS-3 set inconsistent in terms of the volume integral  $J_R/16$  which is large and positive (Table 1). This implies that for a proper analysis, a resonant term in the amplitude needs to be included explicitly. The potentials discussed herein are related to the contribution of scattering due to a mean field only.

The data between 40.77 and 47.3 MeV can again be accounted for using the NMS-2 potential, provided a modest imaginary part is added to it. The parameters are noted in Table 1. The total chi-square in this range is  $\chi_T^2 = 256.6$  which is to be compared with  $\chi_T^2 = 1030.5$  obtained using the BFWC potential.

The reaction cross sections  $\sigma_R$ , calculated using the NMS-2 and NMS-3 sets in the appropriate energy ranges as well as BFWC, are noted in Table 3. Except for a sudden jump in  $\sigma_R$  between 38.83 and 40.77, the reaction cross sections using the NMS potential increases slowly with energy but that is not the case for the BFWC potential.

The real parts of the three NMS potential sets, used in fitting the data from a few MeV to 47.3 MeV, along with the calculated EDF potential are plotted in Fig. 9. As presented in Table 1, the parameters of the NMS-1 potential  $V_0$ ,  $R_0$  and  $a_0$  are very close to those obtained from the EDF theory but the repulsive part of the two differs in magnitude, as expected. On the other hand, the difference between NMS-3 and others is significant. As noted earlier, this might imply

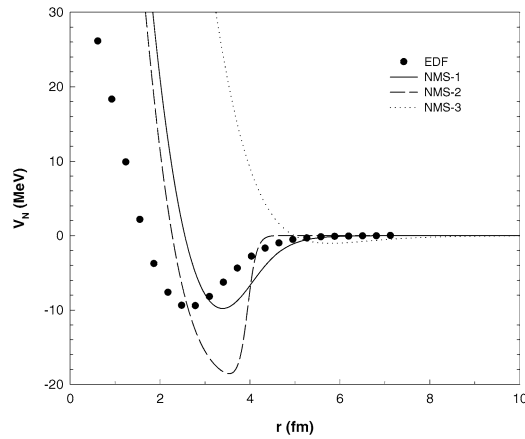


Fig. 9. Non-monotonic shallow potential NMS-1, NMS-2 and NMS-3 sets, noted in Table 1, are compared with the EDF generated potential (solid dots), parametrized in terms of the either  $V_{\text{edf}}(\text{GG})$  or  $V_{\text{edf}}(\text{WG})$  set also in Table 1.

Table 4

Parameters of the non-monotonic complex potential obtained from the best fits of the experimental data at 31.8, 34.2, 35.1, 38.83 and 47.3 MeV. The fits are shown in Fig. 9. All the sets have  $R_C = 5.8$  and  $R_W = 2.5$  fm.  $V_0$ ,  $V_R$  and  $W_0$  are in MeV;  $R_0$ ,  $R_R$  and  $a_0$ , in fm;  $\sigma_R$  in mb, and  $J_R/16$ , in MeV fm<sup>3</sup>

$E_\alpha$	$V_0$	$R_0$	$a_0$	$V_R$	$R_R$	$W_0$	$\sigma_R$	$J_R/16$
31.8	35.0	3.80	0.1	260.0	1.65	0.0	0.0	-99.8
34.2	30.0	3.85	0.97	300.0	2.55	0.0	0.0	963.8
35.1	26.0	3.95	0.97	320.0	2.45	1.613	35.7	972.7
38.83	26.0	3.75	0.77	350.0	2.30	1.613	41.3	974.1
47.3	26.0	3.80	0.25	250.0	1.30	1.613	158.0	-198.3

that a resonance term is to be incorporated explicitly in the analysis. The key difference between the calculated EDF potential and those used in fitting the data is that the short range repulsion of the latter potentials is much stronger. This is the consequence of the difference in the density distribution functions used in the calculation and the actual one near the origin. However, the EDF calculation reproduces the tail of the potential well, which is the determining factor to describe a low energy scattering. The magnitude of the depth of the potential in both cases is about the same but shifted from each other. It is of interest to note that the EDF potential is similar to the one calculated by Thompson et al. [34] using RGM, in particular, in the depth and tail region.

Above the 30 MeV bombarding energy, if one allows the freedom to vary the parameters at every energy, much improved fits to the data can be obtained even around 38 MeV. This is shown in Fig. 10 which compares the data with those calculated using the parameters of the NMS potential listed in Table 4 for 31.8, 34.2, 35.10, 38.83 and 47.3 MeV. Although the fits are very good,  $\sigma_R$  in each case seems to be little different. Despite the variation of the potential parameters, the total real parts of the 31.8, 34.2 and 35.1 MeV potentials resemble one another, as reflected in the potential plot in Fig. 11, and this similarity also applies to the potentials for 38.83 and 47.3 MeV.

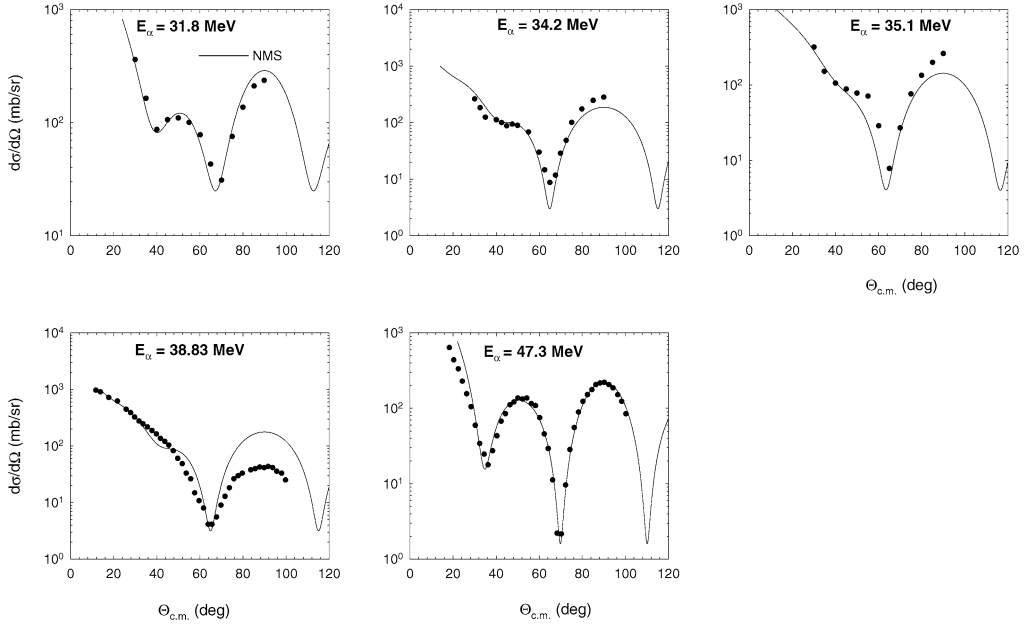


Fig. 10. Comparison of experimental  $\alpha$ - $\alpha$  cross sections for the 31.8, 34.2, 35.1, 38.83 and 47.3 MeV (lab) incident energies in the resonance region with the predictions using the NMS potential parameters in Table 4.

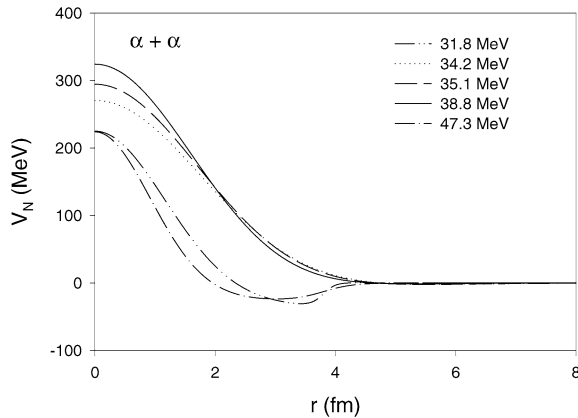


Fig. 11. Real part of the NMS potential using the parameters in Table 4 for the best fits to the data in the resonance region including the 31.8, 34.2, 35.1, 38.8 and 47.3 MeV incident energies.

### 3.2.3. Phase shifts and $^8\text{Be}$ decay width

In a number of investigations, phase shift analyses to the angular distributions up to 47.3 MeV have been performed assuming them to be real. This implies the absence of the loss of incident flux to any but the elastic channel. However, a number of channels other than elastic open up between 35 to 47.3 MeV, implying that a part of the incident flux is lost in these channels. Consequently, allowances for complex phase shifts in the energy region of 35 to 47.3 MeV in the phase shift analyses should be made. Thus, the aforementioned phase shift analyses should be

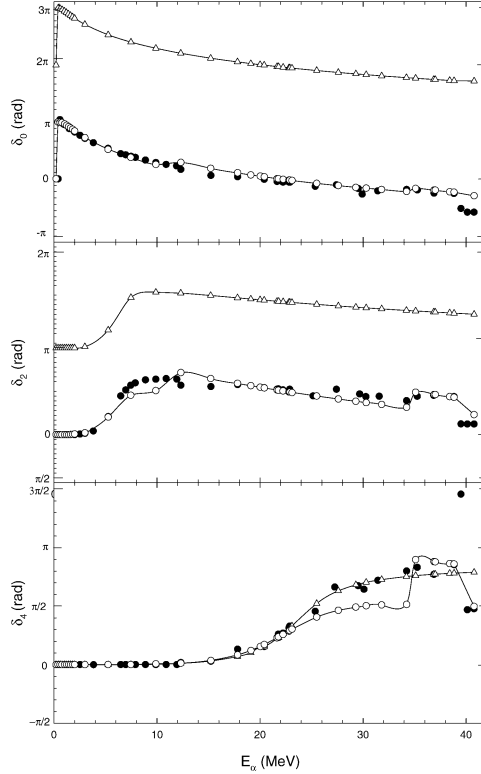


Fig. 12. The  $\alpha$ - $\alpha$  scattering phase shifts, calculated using the deep BFWC (open triangles) and shallow NMS (open circles) potential parameters, are compared with the phase shifts (solid dots) deduced from phase shift analysis of the experimental cross sections.

modified at energies higher than about 35 MeV. In Fig. 12, we have, nevertheless, plotted these phase shifts deduced from the phase shift analyses of the experimental data up to 40 MeV and compared them to the phase shifts calculated using the NMS as well as BFWC potential.

The computed  $s$ -wave phase shift for the NMS-1 potential tends to zero for zero incident energy. In fact, it does not have a bound state. The  $s$ -wave phase shift deduced from the data tends to  $\pi$  at very low energy [65] with no data available below about a few hundred keV. The calculated phase shift using the NMS-1 potential, shown in Fig. 12, tends to zero near zero energy and then jumps to  $\pi$  around 200 keV because of the resonance due to a meta-stable state of  ${}^8\text{Be}$  and then follows closely the deduced  $s$ -wave phase shift.

Thus, for the NMS-1 potential,  ${}^8\text{Be}$  is in a meta-stable state at about the correct energy. The decay width,  $\Gamma$ , of this state can be calculated using the following relation, due to Wigner [66] and Smith [67], between half-life  $T$  and the derivative of phase shift  $\lambda$ , around the resonant energy:

$$T = \hbar/\Gamma = 2\hbar d\lambda(E)/dE. \quad (15)$$

The computed decay width of  $\Gamma = 6.36$  eV agrees very well with the earlier observed value of  $(6.8 \pm 1.7)$  eV [68,69] and the recent value of 5.6 eV obtained from the R-matrix analyses [70]. Above the resonant energy, the calculated  $s$ -wave phase shifts follow closely those deduced from the phase shift analyses as a function of energy, turning negative around 20 MeV bombarding

energy. The negative value of s-wave phase shift is indicative of the short-range repulsion which characterizes the potentials deduced from the EDF calculations and the NMS potential. We may note that the deduced s-, d-, and g-wave phase shifts, however, have structures around 38 MeV [2] which are absent in the calculated ones.

A comparison of 3.0 MeV and 5.26 MeV angular distributions indicates that the d-wave phase shift contributes significantly to the cross section at energies around 5.26 MeV. Because the d-wave has a zero below  $90^\circ$ , the cross section has the observed dip in the 5.26 MeV data. Both the optical model calculations and phase shift analyses indicate that the contribution to the cross section of the d-wave starts becoming significant around 4.0 MeV. Unfortunately, the deduced d-wave phase shifts by [2], [6], and [65] differ from each other in the 6 to 9 MeV energy range and the calculated ones in this energy range are closer to those of [65]. Except for the structure around 38 MeV in the deduced phase shift, the calculated ones reproduce them fairly well. Similarly, the calculated real parts of  $l = 4, 6,$  and  $8$  phase shifts follow closely the ones deduced from the phase shift analyses assuming them not to be complex.

All the deduced  $l = 4, 6,$  and  $8$  phase shifts, from the phase shift analyses [2], tend to zero at zero energy implying that following the Levinson theorem, there should be no  $l = 2, 4,$  and  $6$  bound states in the potential. The computed phase shifts using the NMS potential also tend to be zero at zero energy implying that this shallow potential has no such bound states.

The BFW potential, being a deep one, has two  $l = 0$  and one  $l = 2$  bound states. These states having the configurations 0S, 1S and 0D with the calculated binding energies of 72.6, 25.8 and 22.1 MeV, respectively, in the BFW potential, are asserted by Buck et al. [21] and Neudatchin et al. [20] to be Pauli forbidden (PF) states, in order to explain the discrepancies between the phase-shifts, calculated using their deep potentials, and the actual ones, deduced from the data based phase-shift analysis of the experimental data. Although no actual calculation has been made to determine the number of bound states in the BFWC potential, which, being very similar to the BFW potential in depth and width, is likely to hold the same number of PF bound states. The same holds for the WS parameterization of the BFW potential or the potential of [20].

Both Neudatchin et al. [20] and Buck et al. [21] indicated that the s-wave and d-wave phase shifts for their respective potentials tend to  $3\pi$  and  $\pi$ , respectively, at very low energies and so do these phase shifts of the BFWC potential. Buck et al. also reports the s-wave phase shifts to go to  $2\pi$  as the energy tends to zero. The energy-dependence of  $l = 0$  and  $l = 2$  phase shifts above a few keV energy, calculated from the potential, follows the energy dependence of the deduced ones from the phase shift very well but the s-wave phase shift never becomes negative, although the deduced one for  $l = 0$  from the data based phase-shift analysis is negative above about 20 MeV. The potentials of [20,21], and the BFWC potential, being purely attractive, cannot yield a negative phase shift.

Thus, although the energy dependence of the  $l = 0$  and  $l = 2$  phase shifts calculated from the BFWC potential and the potentials of [20,21] are about the same as the phase shifts deduced from the data and calculated using the NMS potential, they are shifted by  $2\pi$  and  $\pi$ , respectively, for s- and d-partial waves.

#### 3.2.4. Discussion on phase shifts at zero energy

The number of bound states present in a potential can possibly be determined, using Levinson's theorem [43], from the phase shifts in the limit of zero energy for potentials following the

condition

$$\int_0^{\infty} r |V(r)| dr < \infty. \quad (16)$$

Obviously, condition (16) is violated for a potential having a Coulomb component but Ma [71] has ascertained that Levinson's theorem could be extended to the Coulomb case, even though (16) is violated. The consideration of the PF states modifies the Levinson theorem [43]. The inclusion of the Pauli principle leads to an integro-differential equation. For certain types of two-body potential, Swan [72] has shown that the Levinson theorem should be changed to

$$\delta_l(0) - \delta_l(\infty) = (n_l + m_l)\pi. \quad (17)$$

In (17),  $\delta_l(0)$ ,  $\delta_l(\infty)$ ,  $n_l$  and  $m_l$  are, respectively, the phase shifts at zero and infinite energies, the number of bound states in a potential and the number of PF bound states for the  $l$  partial wave. This theorem has been found to be valid in a number of cases where the two-body potential is of the type considered in [72]. For example, the s-wave phase shift of an electron calculated in the Hartree potential of a helium atom tends to  $\pi$  near zero energy [73], but the potential does not have an s-bound state. This is because the number of the PF states, in this case, is one, and Swan's condition holds for this potential. The phase shifts at zero energy for the BFW or a similar potential tend to  $2\pi$  and  $\pi$ , respectively, for the s- and d-wave scattering. Swan's condition, if applicable for this class of potentials, implies two PF s-states and one PF d-state. On the other hand, the potential derived from the EDF theory or the phenomenological NMS potential describing the  $\alpha$ - $\alpha$  scattering does not have PF bound states and interestingly enough supports only one meta-stable state corresponding to the decaying ground state of  ${}^8\text{Be}$  at 92 keV and hence the  $l = 0$  and  $l = 2$  phase shifts are zero near zero (Fig. 12) bombarding energies. This supports not only the experimental facts that both s- and d-states of  ${}^8\text{Be}$  are unbound, but also satisfies Levinson's theorem as well as Swan's condition.

#### 4. Conclusions

We have presented here a non-monotonic shallow potential, the real part of which is based on the potential derived from the EDF theory using a realistic two-nucleon interaction. As shown in Fig. 8, the raw potential, generated from the EDF calculation with limitations (discussed in Section 3.1), reproduces the data at some energies up to 15.2 MeV reasonably well. The NMS potentials, with the NMS-1, NMS-2 and NMS-3 parameter sets, provide an overall good fit to angular distributions for energies up to 47.3 MeV, except in the resonance region, i.e., for energies between 31 to 40 MeV. Although good fits to the data in this energy region can be obtained, if one allows substantial change in parameters at each energy, this leads to the volume integrals for the real part being unusually large positive. To keep consistency in the parameters, it is more reasonable to explicitly add a resonance component [74] to the scattering amplitude to analyze these data. Aside from that, the phase shifts calculated using this potential reproduce those deduced from the phase-shift analyses of the data. The sudden jump in the deduced phase shift around 38 MeV may be indicative of the need to incorporate explicitly a resonance term to the analysis of this data. The calculated s-wave phase shifts above about 20 MeV bombarding energy are negative as deduced from the phase shift analyses of the data. There is no bound state in the potential which is in agreement with the unbound nature of  ${}^8\text{Be}$  and the potential supports a meta-stable s-state at about 100 keV with a decay width of about 6 eV which agrees with the measured half-life of  ${}^8\text{Be}$ .

A slightly modified version of BFW, the BFWC potential with the total  $\chi^2$ ,  $\chi_T^2 = 271.4$ , reproduces the angular distributions up to 31.8 MeV and at 47.3 MeV much better than the parent BFW potential set with  $\chi_T^2 = 2189.7$ . This is in line with the findings of Abdullah et al. [45,46] that a repulsive core in the  $\alpha$ - $\alpha$  potential is needed for the generation of an appropriate folding  $\alpha$ -nucleus potential without a need of renormalization. The non-monotonic NMS potential describes the same experimental data set with  $\chi_T^2 = 948.0$ . The calculated s-wave phase shift from the BFW or BFWC potential is not negative at energies above 20 MeV but the deduced ones and those calculated from NMS are. Whereas the NMS potential reproduces directly the s- and d-wave phase-shifts, obtained from the experimental data, all deep potentials like BFW, BFWC, and WS can reproduce the energy dependence of the phase shifts quite well, although s- and d-wave phase shifts seem to be shifted by  $2\pi$  and  $\pi$ , respectively. It would be very interesting to investigate the phase equivalency in the sense of Bargmann [75,76]. The NMS and the latter deep potentials are all  $l$ -independent.

## Acknowledgements

This work is partially supported by the grants INT-0209583 and INT-0209584 of the US National Science Foundation and a grant from the University Grants Commission, Government of the Peoples' Republic of Bangladesh. The authors thankfully acknowledge the grants. We, thankfully, acknowledge the writers of SCAT2 [61], MINUIT [62] and HARDCORE [63] codes for the permission to use them for this investigation.

## References

- [1] F.E. Steigert, M.B. Sampson, Phys. Rev. 92 (1953) 660.
- [2] P. Darriulat, G. Igo, H.G. Pugh, H.D. Holmgren, Phys. Rev. 137 (1965) B315.
- [3] A.D. Bacher, F.G. Resmini, H.E. Conzett, R. de Swiniarski, H. Meiner, J. Ernst, Phys. Rev. Lett. 29 (1972) 1331.
- [4] R. Nilson, R.O. Kerman, G.R. Briggs, W.K. Jentschke, Phys. Rev. 104 (1956) 1673.
- [5] N.P. Heydenburge, G.M. Temmer, Phys. Rev. 104 (1956) 123.
- [6] T.A. Tombrello, L.S. Senhouse, Phys. Rev. 129 (1963) 2252.
- [7] J.L. Russell, G.C. Phillips, C.W. Reich, Phys. Rev. 104 (1956) 135.
- [8] D.J. Bredin, W.E. Burcham, D. Evans, W.M. Gibson, J.S.C. McKee, D.J. Prowse, J. Rotblat, J.N. Snyder, Proc. R. Soc. London A 251 (1959) 143.
- [9] H.E. Conzet, G. Igo, H.C. Shaw, R.J. Slobodrian, Phys. Rev. 117 (1960) 1075.
- [10] W.S. Chien, R.E. Brown, Phys. Rev. C 10 (1974) 1767.
- [11] A. Nadasen, P.G. Roos, B.G. Glagola, G.J. Mathews, V.E. Viola, H.G. Pugh, P. Frisbee, Phys. Rev. C 18 (1978) 2792.
- [12] K.A.G. Rao, A. Nadasen, D. Sisan, W. Yuhasz, D. Mercer, S.M. Austin, P.G. Roos, R.E. Warner, Phys. Rev. C 62 (2000) 014607.
- [13] R. Nilson, W.K. Jentschke, G.R. Briggs, R.O. Kerman, J.N. Snyder, Phys. Rev. 109 (1958) 850.
- [14] M. Avrigeanu, W. von Oertzen, A.J.M. Plompen, V. Avrigeanu, Nucl. Phys. A 723 (2003) 104.
- [15] J.A. Wheeler, Phys. Rev. 59 (1941) 16.
- [16] S. Ali, A.R. Bodmer, Nucl. Phys. 80 (1966) 99.
- [17] F.C. Barkar, Aust. J. Phys. 22 (1969) 293.
- [18] S.A. Afzal, A.A.Z. Ahmad, S. Ali, Rev. Mod. Phys. 41 (1969) 247.
- [19] R.E. Brown, Y.C. Tang, Nucl. Phys. A 170 (1971) 225.
- [20] V.G. Neudatchin, V.I. Kukulin, V.L. Korotkikh, V.P. Korrenoy, Phys. Lett. B 34 (1971) 581.
- [21] B. Buck, H. Friedrich, C. Wheatley, Nucl. Phys. A 275 (1977) 246.
- [22] H. Horiuchi, Prog. Theor. Phys. 64 (1980) 184.
- [23] R.D. Viollier, G.R. Plattner, D. Trautmann, K. Alder, Phys. Lett. B 40 (1972) 625.
- [24] M. Rahman, S. Ali, S.A. Afzal, Lett. Nuovo Cimento 6 (1973) 107.
- [25] S. Okai, S.C. Park, Phys. Rev. 145 (1966) 787.

- [26] G.R. Satchler, W.G. Love, *Phys. Rep.* 55 (1979) 183.
- [27] G. Spitz, H. Klar, E.W. Schmid, *Z. Phys. A* 322 (1985) 49.
- [28] W. Cassing, S.J. Wang, *Z. Phys. A* 328 (1987) 423.
- [29] D. Krolle, H.J. Assenbaum, C. Funck, K. Langanke, *Phys. Rev. C* 35 (1987) 1631.
- [30] S.A. Sofianos, K.C. Panda, P.E. Hodgson, *J. Phys. G* 19 (1993) 1929.
- [31] A. Lumbroso, *Phys. Rev. C* 10 (1974) 1271.
- [32] J. Griffin, J.A. Wheeler, *Phys. Rev.* 108 (1957) 311.
- [33] R. Beck, J. Borysowicz, D.M. Brink, M.V. Mihailovic, *Nucl. Phys. A* 244 (1975) 58.
- [34] D.R. Thompson, I. Reichstein, W. McClure, Y.C. Tang, *Phys. Rev.* 185 (1969) 1351.
- [35] I. Reichstein, Y.C. Tang, *Nucl. Phys. A* 139 (1969) 144.
- [36] S. Saito, *Prog. Theor. Phys.* 41 (1969) 705.
- [37] W.R. Coker, T. Tamura, *Phys. Lett. B* 62 (1976) 374.
- [38] H. Friedrich, L.F. Canto, *Nucl. Phys. A* 291 (1977) 249.
- [39] D.R. Thompson, M. LeMere, Y.C. Tang, *Nucl. Phys. A* 286 (1977) 53.
- [40] K.R.S. Devi, M.R. Strayer, J.M. Irvin, *J. Phys. G* 5 (1979) 281.
- [41] D. Baye, *Phys. Rev. Lett.* 58 (1987) 2738.
- [42] E.F. Hefter, K.A. Gridnev, *Prog. Theor. Phys.* 72 (1984) 549.
- [43] N. Levinson, K. Dan. Vidensk. Selsk. Mat. Fys. Medd. 25 (9) (1949).
- [44] W.E. Burcham, G.P. McCauley, D. Berdin, W.M. Gibson, D.J. Prowse, J. Rotblatt, *Nucl. Phys. A* 5 (1958) 141.
- [45] M.N.A. Abdullah, S. Hossain, M.S.I. Sarker, S.K. Das, A.S.B. Tariq, M.A. Uddin, A.K. Basak, S. Ali, H.M. Sen Gupta, F.B. Malik, *Eur. Phys. J. A* 18 (2003) 65.
- [46] M.N.A. Abdullah, M.S.I. Sarker, S. Hossain, S.K. Das, M.A. Uddin, A.S.B. Tariq, A.S. Mondal, A.K. Basak, S. Ali, H.M. Sen Gupta, F.B. Malik, *Phys. Lett. B* 571 (2003) 41.
- [47] G. Bertsch, J. Borysowicz, H. McManus, W.G. Love, *Nucl. Phys. A* 284 (1977) 399.
- [48] K.A. Brueckner, S. Coon, J. Dabrowski, *Phys. Rev.* 168 (1968) 1184.
- [49] I. Reichstein, F.B. Malik, *Phys. Lett. B* 37 (1971) 344.
- [50] P. Manngård, M. Brenner, M.M. Alam, I. Reichstein, F.B. Malik, *Nucl. Phys. A* 504 (1989) 130.
- [51] M.N.A. Abdullah, A.B. Idris, A.S.B. Tariq, M.S. Islam, S.K. Das, M.A. Uddin, A.S. Mondal, A.K. Basak, I. Reichstein, H.M. Sen Gupta, F.B. Malik, *Nucl. Phys. A* 760 (2005) 40.
- [52] M.S. Billah, M.N.A. Abdullah, S.K. Das, M.A. Uddin, A.K. Basak, I. Reichstein, H.M. Sen Gupta, F.B. Malik, *Nucl. Phys. A* 762 (2005) 50.
- [53] L.R.B. Elton, *Nuclear Sizes*, Oxford Univ. Press, London, 1961.
- [54] K. Brueckner, S. Coon, J. Dabrowski, *Phys. Rev.* 168 (1968) 1184.
- [55] M.A. Hooshyar, I. Reichstein, F.B. Malik, *Nuclear Fission and Cluster Radioactivity*, Springer-Verlag, Berlin, 2005.
- [56] M.A. Nagarajan, C. Mahaux, G.R. Satchler, *Phys. Rev. Lett.* 54 (1985) 1136.
- [57] C. Mahaux, H. Ngô, G.R. Satchler, *Nucl. Phys. A* 449 (1986) 354.
- [58] H. de Vries, C.W. de Jager, C. de Vries, *At. Data Nucl. Data Tables* 36 (1987) 496.
- [59] D. Baye, L. Desorgher, D. Guillaín, D. Herschkowitz, *Phys. Rev. C* 54 (1996) 2563.
- [60] A.S.B. Tariq, A.F.M.M. Rahman, S.K. Das, A.S. Mondal, M.A. Uddin, A.K. Basak, H.M. Sen Gupta, F.B. Malik, *Phys. Rev. C* 59 (1999) 2558.
- [61] O. Bersillon, SCAT2 code, NEA 0829, 1988.
- [62] F. James, M. Roos, *Comput. Phys. Commun.* 10 (1975) 343.
- [63] L. Rickertsen, F.B. Malik, *HARDCORE Code*, Yale University, New Haven, Connecticut, USA, 1969.
- [64] P. Mohr, T. Rauscher, H. Oberhammer, Z. Máté, Zs. Fülöp, E. Somorjai, M. Jaeger, G. Staudt, *Phys. Rev. C* 55 (1997) 1523.
- [65] C.M. Jones, G.C. Phillips, P.D. Miller, *Phys. Rev.* 117 (1960) 525.
- [66] E.P. Wigner, *Phys. Rev.* 98 (1955) 145.
- [67] F.T. Smith, *Phys. Rev.* 118 (1960) 349.
- [68] T. Lauritsen, F. Ajzenberg-Selove, *Nucl. Phys.* 78 (1966) 1.
- [69] J. Benn, F.B. Dally, H.H. Miller, R.F. Pixley, H.H. Staub, H. Winkler, *Phys. Lett.* 20 (1966) 43.
- [70] P.R. Page, *Phys. Rev. C* 72 (2005) 0541312.
- [71] Z.-Q. Ma, *Phys. Rev. D* 33 (1986) 1745.
- [72] P. Swan, *Proc. R. Soc. London A* 228 (1955) 10.
- [73] F.B. Malik, E. Trefftz, *Z. Naturforsch.* 16a (1961) 492.
- [74] M. Brenner, et al., *Heavy Ion Phys.* 2 (1995) 269.
- [75] V. Bargmann, *Phys. Rev.* 75 (1949) 301.
- [76] V. Bargmann, *Rev. Mod. Phys.* 21 (1949) 488.